Fungal Biology 130 (2026) 101749

Contents lists available at ScienceDirect

Fungal Biology

journal homepage: www.elsevier.com/locate/funbio

Raman spectroscopy in microfluidic chips reveals hyphal scale stress-associated metabolic responses in filamentous soil fungi

Milda Pucetaite [a,*], Paola M. Mafla-Endara [a,b], Yitsully G. González [a], Hanbang Zou [a], Robert W. Schmidt [c], Freek Ariese [c], Edith C. Hammer [a]

[a] Department of Biology, Lund University, Sweden
[b] Department of Forest Mycology and Plant Pathology; Division of Forest Microbiology, Swedish University of Agricultural Sciences, Uppsala, Sweden
[c] LaserLaB, Department of Physics and Astronomy, Vrije Universiteit Amsterdam, the Netherlands

ARTICLE INFO

Keywords:
Raman scattering microspectroscopy
Stable-isotope probing
Soil fungi
metabolic activity
Microfluidic chips
Stimulated Raman scattering (SRS) microscopy

ABSTRACT

Understanding metabolic processes of soil fungi is essential for elucidating their ecological roles in biogeochemical cycles and responses to emergent environmental stressors. Here, we demonstrate the potential of using stable isotope probing Raman (SIP-Raman) microspectroscopy in microfluidics technology-based soil chips to trace glucose metabolism rates and stress responses in laboratory grown filamentous soil fungus *Psilocybe cf. subviscida*. The time evolution of Raman spectral band intensities resulting from deuterated glucose uptake in the fungal hyphae allowed us to assess glucose metabolism rates. Under excess copper (Cu) stress, we observed suppression of both glucose metabolic activity and growth. In addition, reduced spectral signatures of intracellular cytochrome *c* further implied impaired mitochondrial function and potential onset of cell death. However, laser-induced radiation damage hampered repeated Raman measurements, including multispectral mapping, on individual hyphae, especially when exposed to the Cu stress. To overcome this, we employed stimulated Raman scattering (SRS) microscopy, which offers much higher sensitivity and mapping speeds, and therefore much lower radiation doses. This enabled localization of the uptaken glucose at the inner edges of the *P. cf. subviscida* hyphae and Cu-induced formation of putative vacuolar structures. While integration of this approach with soil chips requires future modifications to the chip design for increased optical transparency and ensured sterility, overall, our results demonstrate the potential of Raman-based microspectroscopy for spatially resolved, *in situ* analysis of fungal primary metabolism and stress physiology.

1. Introduction

Metabolic performance of soil fungi is an essential determinant in terrestrial biogeochemical cycles. Catabolic processes are responsible for decomposition, nutrient release, and respiration, while anabolic processes result in biomass growth and production of metabolites. Both are important parameters in estimating carbon (C) and other nutrient cycling (Bölscher et al., 2024), but also for describing overall functioning and fitness of organisms in changing environments.

In bulk soil samples, metabolic performance of microbes can be indirectly analysed via measurements of CO_2 emissions (respiration, substrate consumption) and incorporation rates of tracer molecules such as stable or radioactive isotopes into the biomass (growth) (Rousk and Bååth, 2011). Fungal growth specifically can be measured via, for example, incorporation of isotope-labelled compounds into ergosterol, a lipid found in cellular membranes of fungi (Rousk and Bååth, 2011). Overall, the bulk measurements provide important information about community level fungal responses to changing environmental conditions, although studies of non-growth anabolic activity, such as the production of extracellular metabolites, have been more challenging (Redmile-Gordon et al., 2014).

While laboratory studies conducted on agar plates do not account for numerous factors present in natural environments, they also yield valuable insights into the metabolic responses of mycelia at culture level (Camenzind et al., 2025; Costa and Nahas, 2012). However, fungal hyphae in the mycelium display phenotypical heterogeneity and differ in their function and activity levels (Hewitt et al., 2016; Op De Beeck et al., 2020; Zacchetti et al., 2018). Furthermore, microbes have been shown to individually respond to their immediate microenvironment (Calabrese et al., 2021; Xiong et al., 2022), which may be particularly

* Corresponding author.
E-mail address: milda.pucetaite@biol.lu.se (M. Pucetaite).

https://doi.org/10.1016/j.funbio.2026.101749
Received 27 October 2025; Received in revised form 16 February 2026; Accepted 4 March 2026
Available online 13 March 2026

important for filamentous fungi that extend their hyphae through spatially and temporally heterogeneous environments of soil when foraging for nutrients. Therefore, deeper insights into the fundamental processes governing fungal metabolic performance can be obtained by also studying them at a single-hypha level (Hatzenpichler et al., 2020).

Nanoscale secondary ion mass spectrometry (nanoSIMS) has enabled measurements of single-cell anabolic activity in both cultured and uncultured microbes via stable-isotope probing (SIP) (Gao et al., 2016). Fluorescent RNA (Joux and Lebaron, 2000) or newly synthesized protein tags (Hatzenpichler and Orphan, 2016) and single-cell transcriptomics (Imdahl et al., 2020) have been used to track phenotypic variation in microbial communities as a response to stressors. These approaches, however, have limitations. Namely, the fluorescent RNA tagging can only be applied to a limited number of laboratory-grown species and target single genes, while the use of bio-orthogonal non-canonical amino acid tagging (BONCAT) for monitoring newly synthesized proteins is limited to microbes that are capable of taking up the synthetic amino acids, which can also be toxic for some taxa (Hou et al., 2025). Meanwhile, nanoSIMS and single-cell transcriptomics are destructive, which means that observations *in vivo* are impossible.

Recently, Raman scattering microspectroscopy combined with SIP has been introduced as a novel approach to trace single-cell level anabolic activity of environmental microbes (Alcolombri et al., 2022; Berry et al., 2015; Schaible et al., 2022). This method is non-destructive as long as radiation damage is avoided by maintaining low laser excitation power and limited exposure, allowing for live monitoring of microbial metabolic processes over time (Yasuda et al., 2021). Tracing of stable isotopes is done via peak position shifts of spectral bands associated with molecular vibrations involving the isotopes. The shift is related to the mass ratio between the isotopes, which means that the largest shift values are observed for deuterium (^{2}H). This, and the fact that the bands associated with νC-^{2}H stretching vibrations are located in the 'silent region' of a Raman spectrum, between 1800 and 2700 cm^{-1}, makes the use of ^{2}H labelled substances particularly suitable for sensitive tracing of associated metabolisms. For example, ^2H_2O has been used for overall anabolic activity measurements of microbes (Berry et al., 2015; Omelchenko et al., 2023), while ^{2}H labelled glucose or other carbon sources have been applied for studying their metabolism specifically (Xu et al., 2017; Yasuda et al., 2021). Compounds enriched with ^{13}C or ^{15}N and their combinations have also been used (Cui et al., 2023), but care has to be taken when interpreting the results, as the spectral band shifts are smaller and incorporation of the labels into multiple different compounds can cause complex changes in the recorded spectra (Ivleva et al., 2017). Finally, the reverse labelling approach using in advance SIP labelled microbial cultures can help determine metabolic rates of more complex substrates when the signal of the SIP is being lost during incorporation of the unlabelled compounds (Wang et al., 2016).

Whereas the majority of SIP-Raman microspectroscopy applications have been performed on bacterial samples, Yasuda et al. investigated the potential of using ^{2}H labelled glucose for tracing its metabolism in filamentous soil fungus *Aspergilus nidulans* (Yasuda et al., 2021). Spectral mapping further revealed glucose accumulation along the inner edges of the analysed cells, followed by incorporation of deuterium from glucose into newly synthesized proteins in the central part of the hyphal tips.

Another advantage of Raman microspectroscopy is the possibility to trace other unlabelled molecular compounds within microbial cells. Spectral differences and changes within the cells can be species specific or indicate phenotypical alterations as a response to environmental pressures (No et al., 2022). All in all, although Raman microspectroscopy of microbial samples, particularly at the single-cell level, can be challenging due to low scattering cross-sections and potential interference by fluorescence (Butler et al., 2016), it is a promising approach for tracing soil microbial metabolic processes *in situ*. For this, a combination of Raman microspectroscopy with microfluidics-based *soil chips* can be particularly useful (Pucetaite et al., 2021), as cells and hyphae can be singled out into one focal plane while still being connected to their culture or community.

Applications of microfluidic technology in soil microbial ecology have recently opened up possibilities for studying growth and functioning of living soil organisms at the microscale (Aleklett et al., 2018; E. Stanley et al., 2016; Mafla-Endara et al., 2021; Richter et al., 2022). These soil chips constitute a set of interconnected microchannels etched or engraved into an optically transparent material and serve as habitats for the microbes that are inoculated within the chip. Although artificial, they can be set up at a structural and chemical complexity level that allows mimicking real ecosystems. Metabolic activity of fungal cells growing within has been analysed using fluorescent markers (Arellano-Caicedo et al., 2021; Gimeno et al., 2021; Mafla-Endara et al., 2023), but higher chemical specificity can be offered by Raman microspectroscopy, which can be performed in chip channels without any additional modifications to its design (Cui et al., 2023; F. Chrimes et al., 2013; Pucetaite et al., 2021).

Here, we demonstrate the potential of using Raman microspectroscopy in soil chips to estimate anabolic glucose metabolism rates of laboratory grown soil fungus *Psilocybe cf. subviscida* and its biochemical response to a stressor, which in this study was implemented as addition of copper (Cu) in the form of hydrous Cu sulphate. The fungus was chosen due to its relatively fast growth rates and non-pigmented mycelium, which does not produce fluorescence when recording the Raman spectra. Meanwhile, Cu is an essential micronutrient, which, when in excess, produces well-described dose-dependent toxic effects (Robinson et al., 2021). Here, Cu was thus introduced as an easy-to-control stressor at a concentration level sufficient to reduce the fungal growth rates but low enough to avoid immediate fatality. We found that not only can the metabolic rates be traced at a single-cell level in living fungal hyphae by following the stable-isotope (^{2}H) labelled glucose uptake over time, but the biochemical effects of the stressor can be identified via analysis of the Raman spectra recorded at the hyphal tips. Specifically, we hypothesized that the environmental stimulus (in this case Cu) will shift hyphal metabolism from growth oriented to 'adaptation' oriented, which will have an effect on the growth rates, glucose incorporation rates and chemical signature of newly synthesized cellular compounds. The soil chips provide a structural, optically available habitat for the fungi that can be set up for sterile measurements over time. The chip channels, in addition to separating individual hyphae from the bulk mycelium, provide an internal replication system.

We also demonstrate, as a proof-of-principle, the use of stimulated Raman scattering (SRS) microscopy for chemical mapping of the selected chemical components in fungal hyphae in soil chips. Narrowband SRS makes use of two synchronized picosecond laser beams of which the photon energy difference is tuned to a specific molecular vibration of the target compound (Nandakumar et al., 2009). As the intensity of SRS is much higher than that of the conventional (spontaneous) Raman effect, the mapping speed can be more than 3 orders of magnitude higher (Zada et al., 2021), but at the cost of spectral information: only a single vibrational energy is monitored at the time. For additional chemical selectivity, this can be repeated at a few other specific wavenumber settings and hyperspectral images can be constructed. Alternatively, broadband, femtosecond laser sources can also be used for hyperspectral SRS microscopy, where the SRS signal can be recorded over a range of vibrations simultaneously, though cross phase modulation can be an issue (Würthwein et al., 2020). With continuous improvements on the spectral range width and achievable spectral resolution (Figueroa et al., 2018; Fu et al., 2013), these systems are also becoming more widespread. One major reason for testing (picosecond) SRS for our samples was the fact that the much greater mapping speeds

would result in much lower radiation doses, which in the case of spontaneous Raman mapping had been found to affect the hyphae.

2. Materials and Methods

2.1. Soil chip preparation

The microfluidic chips used in this work were made by moulding polydimethylsiloxane (PDMS) on a master fabricated by maskless lithography. Briefly, negative photoresist mr-DWL 5 (micro resist technology GmbH, Berlin, Germany) was spin coated onto a silicon wafer, followed by patterning with a fabricated MLA150 Maskless Aligner (Heidelberg Instruments Mikrotechnik GmbH, Heidelberg, Germany). To facilitate de-moulding, all masters were coated with a self-assembled monolayer (SAM) of perfluorodecyltrichlorosilane (FDTS) using a Fiji ALD system (Veeco, Plainview, New York, United States). The PDMS was prepared by mixing a PDMS base with a curing agent (Sylgard, 184, Dow Corning, USA) at a 10 to 1 (m/m) ratio. The mixture was then cast over the prepared master to approx. 5 mm thickness, degassed at approx. −0.8 - -1 kPa until no air bubbles remained (2 - 3 h) and cured in an oven at 70 °C for at least 2.5 h.

The chip design (SI Fig. 1), adapted from (Mafla-Endara et al., 2023), consists of 68 straight channels, each 10 μm wide and 20 mm long. Along the channels, 58 diamond-shaped expansions (140 μm in diameter, spaced 200 μm apart) are incorporated. Half of the channels (34) connect at both ends to entrance regions supported by circular pillars (100 μm in diameter, 75 μm spacing), whereas the remaining channels connect to only one entrance region, with the opposite end closed. The partially blocked and the fully open channels are randomly distributed across the chip. In this work, only the fungal hyphae growing in the fully open channels were monitored. The entrance area was used for cutting the chip open for addition of growth medium and inoculation of fungal culture as described below. The total dimensions of the chip are 2.5 cm long and 1.47 cm wide, with an internal height of 11 μm.

After curing, PDMS slabs were cut around the microstructures with a scalpel and peeled from the master. Two openings to the chip were introduced in the entrance areas using a 2.5 × 5 mm leather punch. Then, the slabs were plasma bonded to a custom-made glass cover slip-bottomed Petri dish (60 mm diameter, 8 mm height), as described in (Arellano-Caicedo et al., 2021). Prior to use, the prepared chips were sterilized by exposure to UV radiation for 30 min in a sterile laminar flow hood.

2.2. Fungal cultures and treatments

Laboratory cultures of saprotrophic soil fungus *Psilocybe cf. subviscida* (CBS101986) were maintained in malt extract growth medium and transferred to a Highley (1973) medium before further experiments in the soil chips. Fungal cultures were used for soil chip inoculation as described below after 10 days of incubation in Highley medium, at which point the mycelium reached approximately half of the Petri plate radius.

Immediately after fabrication and sterilization, the soil chips were filled with 160 μl of liquid Highley medium by pipetting 80 μl of the medium into each of the two openings. A ~2.5 × 5 mm piece of agar was cut out from the forefront of the fungal mycelium in the Petri plate cultures. It was placed in one of the chip openings with the mycelium facing down and its growth direction - towards the chip channels. The fungus was then left to colonize the chip for 7 days in the dark at 21 °C.

After the incubation period, the liquid medium from the entrance without fungal inoculum was removed using a pipette and filled with 80 μl of treatment solutions. For controls, an aqueous 8 g/l solution of deuterated glucose (D-glucose-1, 2, 3, 4, 5, 6, 6-d_7, Merck, CAS 23403-54-5; further glucose-d_7) was used. We considered that after its diffusion into the chip channels, and dilution of the remaining initial medium, the resulting concentration of deuterated glucose was 4 g/l (21 mM). For the Cu treatment, 80 μl aqueous solution of 21 mM glucose-d_7 and 1 mM of $CuSO_4 \bullet 5H_2O$ (for a final concentration of 0.5 mM) was introduced into the chip instead. To determine the Cu concentration level for the experiments, *P. cf. subviscida* was grown in Highley medium agar cultures on Petri plates at 0, 0.1, 0.5, 1 and 2 mM $CuSO_4 \bullet 5H_2O$ for 2 weeks at 21 °C in the dark (data not shown), and 0.5 mM final concentration was selected as one that significantly reduced, but not fully suppressed the fungal growth. Eight fungi inoculated chips were prepared, four replicates for the two treatments described above.

To evaluate the potential effects of the SIP glucose on the growth rates of *P. cf. subviscida* hyphae, additional fungus-inoculated chip samples were prepared as described above, but both control and Cu treatments contained either non-deuterated glucose or glucose-d_7. Three replicates for each of the four resulting treatments were made.

2.3. Optical microscopy

Optical microscopy images before the introduction of the treatments (0 h) and at 4 h, 20 h, 28 h and 50 h after it were acquired using a Nikon Ti2-E inverted microscope and the software NIS-Elements. The ND Acquisition mode was used to obtain the images: large ones comprising all 68 channels covering the maximum length reached by the hyphae and detailed pictures of three randomly selected channels. For the large field-of-view images, the CFI Plan Fluor × 20/0.45, 2.1 mm working distance (W. D.) objective was used. The composite image of a chip was obtained by stitching individual images collected over the whole chip width, and the length varying according to the length of the hyphae at the time of measurement. For better visualization of hyphal morphology and traceability of growth, detailed high-resolution images from the selected hyphae were recorded using a CFI Plan Apochromat DM Lambda × 40/0.95, 0.21 mm W. D. objective.

2.4. Raman microspectroscopy

Raman scattering measurements were performed in the soil chips before the introduction of glucose-d_7 and Cu treatments (T_0) and at 9 h (T_9), 20 h (T_{20}), 28 h (T_{28}) and 46 h (T_{46}) after labelling, using an upright confocal Raman microspectroscopy system (LabRAM HR Evolution, Horiba) equipped with a 532 nm laser source (P_{max} = 750 mW), 600 Gr/mm grating and back-illumination deep thermoelectrically-cooled CCD detector (Syncerity, Horiba Scientific). The samples were placed on a motorized xyz-stage with the glass coverslip of the Petri plates containing the soil chips facing the objective (SI Fig. 2). Raman spectra were recorded in 180° (back scattering) geometry via the glass coverslip (~170 μm thick) using an oil immersion Olympus Plan N 100 × /1.25 objective and a 50 % transmission neutral density (ND) filter limiting the power of incoming laser beam at the sample. Then, measured power at sample was $P_{at\ sample}$ = 6.3 mW. The spectra were collected over the 450-3750 cm^{-1} spectral range. The confocal hole was set to 50 μm diameter to limit the contribution of chip constituent materials (PDMS and glass) to the spectra. Each spectrum recorded at the first 5 μm of a hyphal tip (the most metabolically active part of fungal cells) was followed by a measurement of a spot directly adjacent to it, which was used as a background for subtraction of the remaining spectral bands originating from the chip constituent materials as well as water in the growth medium.

For identification of hyphal biochemical signatures, Raman spectra were recorded from at least 3 individual hyphae at the growth front in the channels at the time points indicated above (1 s exposure, 32 acquisitions were averaged for each spectrum; for collection of a full spectrum, four rotations of the diffraction grating were required, thus resulting in a total collection time per spectrum t = 128 s). A reference spectrum of 80 g/l glucose-d_7 solution in a separately prepared chip was recorded using the same acquisition parameters. For monitoring the glucose-d_7 metabolism rates, Raman spectra were recorded on at least 10 other individual hyphae using a reduced total laser exposure time

(0.5 s exposure, 16 acquisitions were averaged, total collection time per spectrum $t = 32$ s) in order to reduce radiation damage observed during the measurements of longer exposure. Raman spectra at the subsequent time points were recorded on the same fungal hyphae, unless there were visible radiation damage effects. In this case, a new hypha in either the same or a different channel was selected. Throughout the experiment time, 5 hyphae in each of the analysed chips were selected and their growth rates monitored without exposure to the laser radiation in order to evaluate the radiation damage effects. Of note, due to limitations on the time required to record spectra in multiple chips and on multiple hyphae, pairs of replicate chips were prepared and analysed on different days. Furthermore, a lower number of hyphae grew into the chip's channels in one of the replicates, which yielded fewer recorded Raman spectra.

Raman spectral mapping was performed on selected hyphae before and 1 day after glucose-d_7 addition in control treatment chips. The maps were collected within a selected area of the hyphal tips with the same spectral acquisition parameters as above (total acquisition time $t = 32$ s) and at 0.3 μm step size.

2.5. Stimulated Raman scattering (SRS) microscopy

As part of a pilot study, we further performed spectral imaging of *P. cf. subviscida* hyphae growing in the soil chips using stimulated Raman scattering (SRS) microscopy at LaserLaB Amsterdam. The images in both control and Cu treatments were recorded 1 d after glucose-d_7 or glucose-d_7 with Cu addition using a custom-built SRS system as previously described in (van Haasterecht et al., 2020). Briefly, a frequency-doubled 532 nm beam from a picosecond Lumera Plecter Duo Nd:YAG laser was used to pump a Levante Emerald Optical Parametric Oscillator (OPO), while the 1064 nm beam from the same laser was sent onto a delay stage and to an Acousto-Optical Modulator at 3.636 MHz from EQ Photonics GmbH. The OPO (Pump beam) was tuned so that the photon energy difference with the fixed 1064 nm beam (Stokes) would correspond with the targeted molecular vibrations: the νC-H spectral band (811 nm corresponding to Raman shift 2932 cm^{-1}) and at several wavenumbers of the νC-^{2}H spectral range (867.4, 865.6, 864.4, 861.4 nm corresponding to 2130, 2154, 2170, 2207 cm^{-1} respectively). We also recorded off-resonance SRS images at 893 nm corresponding to Raman shift 1800 cm^{-1}. Then both beams were spatially overlaid with the help of a dichroic mirror and sent to a Zeiss Examiner 7 MP laser scanning microscope equipped with a Zeiss C-Achroplan W 32 × /0.85 water immersion objective and a water immersion condenser with a numerical aperture of 1.2. For detection, a DET36A photodetector from Thorlabs was used in transmission geometry, and the signal was demodulated with a lock-in amplifier from Zurich Instruments. SRS scans were acquired through Zeiss's ZEN2011 microscope software with a step size of 120 - 150 nm and a pixel dwell time of 177 μs. Eight scans were averaged for a final image. Typical laser powers (at the sample) were 9 mW for the Pump and 11 mW for the Stokes beam. The effective SRS spot size of the setup had been determined in a previous study as 0.67 μm (Zada et al., 2021).

2.6. Data analysis

In the three replicate chips prepared for optical microscopy experiments as described above, we estimated growth rates of randomly selected *P. cf. subviscida* hyphae in 3 separate channels. The NIS Element Viewer software v. 5.21.00, was used for visualization and measurement of the hyphal elongation between the subsequent time points using the chip's internal ruler and the software distance measurement tool. Total elongation and growth rates (μm/hour) at each time point were then calculated.

Raman spectra recorded with a longer exposure time were pre-processed by subtracting the spectrum of the background medium from the spectrum of the hyphae (no scaling was applied to the background spectrum). The subtracted spectra were then truncated to 500 – 3030 cm^{-1} spectral range, smoothed using a Savitzky-Golay digital filter (polynomial of degree 2 and window size 21), baseline corrected (linear baseline through first and last points) and vector normalized. Spectra of 5 individual hyphae at each time point were averaged for further inspection of the spectral bands. Further, the averaged spectra at T46 were truncated to the νC-^{2}H associated spectral range (2000 – 2500 cm^{-1}), baseline corrected (as above), min-max normalized and fitted with four Voigt functions, with their parameters (peak position, peak intensity and peak width) optimized by least-square minimization. Initial fit parameters were set according to the four νC-^{2}H bands of the glucose-d_7 spectrum (Omelchenko et al., 2025).

For glucose-d_7 uptake rates analysis, Raman spectra recorded with a shorter exposure time were pre-processed as described above, but skipping the background medium subtraction step. Spectra of low quality in terms of signal-to-noise ratio were manually removed, leaving 21-28 data points for each time point. Then, the integral intensity of the νC-^{2}H band in the 2050 – 2350 cm^{-1} spectral range was calculated and divided by the integral intensity of the δC-H spectral band in the 1432-1485 cm^{-1} range. This ratio represents relative deuterium enrichment in the hypha.

Raman spectra in multispectral maps were pre-processed by subtracting the spectrum of the background medium followed by truncating to the 1200 – 2400 cm^{-1} spectral range, smoothed using a Savitzky-Golay digital filter (polynomial of degree 2 and window size 21), baseline corrected (rubber band) and vector normalized. The reference spectrum of the background medium for subtraction was obtained by averaging three randomly selected spectra from the map in the area off the hypha. Raman chemical images were obtained by calculating and plotting the integral intensity of selected Raman bands: amide I (1643-1683 cm^{-1}) and C-^{2}H (2060-2280 cm^{-1}), divided by the integral intensity at the baseline (1501-1525 cm^{-1} or 1900-1925 cm^{-1}). All the spectral analysis was performed using Quasar version 1.10.2 (Toplak et al., 2017, 2021), and for visualization of the spectra we used graphing software OriginPro version 2025 (OriginLab Corporation, Northampton, MA, USA).

SRS images collected at the νC-H spectral band were pre-processed using Matlab (version R2023b for Windows, MathWorks) script for BM3D denoising (Dabov et al., 2007; Mäkinen et al., 2020). Residual background was subtracted using the rolling ball algorithm in Image J v. 1.53q (Schneider et al., 2012), with the radius of the rolling ball set to 10 or 30. The SRS signal of the images collected at the νC-^{2}H band was too low and such denoising did not yield satisfactory results; therefore, they are shown as raw data. When necessary, regular diagonal noise appearing in some images was removed using Fourier transform filtering (ImageJ).

Statistical analysis was performed in Origin Pro (2025) software using analysis of variance (ANOVA) with Tuckey's test as the post hoc test. Normality of variance of residuals was tested using Shapiro–Wilk test. When the normality test failed, log transformation was applied to the data and the analysis performed again.

3. Results

The fungus *P. cf. subviscida* was grown in soil chips in both Highley medium supplemented with 21 mM glucose or glucose enriched with deuterium (glucose-d_7), to test for any potential effects of the deuterium as SIP on the hyphal growth rates (SI Fig. 3), and in full factorial manner - with or without added $CuSO_4 \bullet 7H_20$ (0.5 mM). Three replicate chips for each treatment were prepared and analysed. We did not observe any significant differences in the total elongation or growth rates of hyphae between the regular glucose and glucose-d_7 treatments. Although the variation in growth of individual hyphae within and across replicate chips was high, generally the total elongation and growth rates of hyphae were lower in the Cu compared to no-Cu treatments. The variation across the chips also resulted in non-significant differences between the

two Cu-treatments.

We then recorded Raman spectra of the *P. cf. subviscida* hyphae growing in the soil chips before and during 46 h following addition of glucose-d_7 or a solution of glucose-d_7 with $CuSO_4 \bullet 5H_2O$ (0.5 mM). The average spectra from 5 hyphal tips for each treatment and at each time point (0 h (before treatment addition), 9 h, 20 h, 28 h, and 46 h) are presented in Fig. 1. A spectrum of the surrounding growth medium was recorded adjacent to each hypha and subtracted from each spectrum recorded on the hypha to eliminate the influence of water in the channels and PDMS (SI Fig. 4). When possible, spectra at subsequent time points were recorded on the same fungal hyphae; however, repeated laser exposure consistently resulted in hyphal damage, with halted growth, cytoplasm spillage and other morphological changes observed. Radiation exposure had a stronger effect on hyphae growing under Cu treatment (SI Fig. 5), and further lowering exposure time or laser power was not possible due to too low signal-to-noise ratio of the recorded spectra. Therefore, each time point sampled a different set of individual hyphae, providing a 'snapshot' of fungal organismal response and changes in glucose metabolism in control and Cu treatments.

At time 0 h, the most prominent spectral bands in the fingerprint region (500 – 1800 cm^{-1} spectral range) are assigned to proteins: amide I (dominated by νC=O vibrations) at 1657 cm^{-1} and amide III (dominated by νC-N and δN-H vibrations) at ~1234 cm^{-1}, and resonant Raman bands of reduced cytochrome *c*: 1583 cm^{-1}, 1316 cm^{-1}, 1127 cm^{-1} and 748 cm^{-1} (Mucha, 2011). The band at 1443 cm^{-1} is assigned to δC-H vibrations, while intense spectral band peaking at 2931 cm^{-1} is assigned to νC-H vibrations in the organic compounds of the fungal cells. Weak spectral bands at 1604 cm^{-1} (not marked in Fig. 1) and 1003 cm^{-1} are assigned to ring νC=C and benzene ring breathing vibrations in phenylalanine, respectively. Of note, the cytochrome *c* related bands in the hyphae grown under Cu treatment conditions diminished and disappeared completely during the 46 h measurement period, while generally remaining unaffected in the hyphae grown in the controls.

After addition of the treatments and as the hyphae were metabolizing glucose-d_7 during the 46 h time period, a spectral band appeared in the cells, peaking at ~2170 cm^{-1} and assigned to νC-^{2}H vibrations in newly synthesized organic compounds. The intensity of this band increased at each subsequent time point as more ^{2}H was incorporated into the hyphal compounds from metabolized glucose. Closer inspection and band fitting revealed structural differences, including shifts in the peak positions and/or changes in their relative intensities, between spectra of glucose-d_7 in aqueous solution and the spectra of hyphae in the control and Cu treatments after 46 h (Fig. 2, SI Table 1). This confirms that the νC-^{2}H bands in the Raman spectra of the hyphae stem from compounds newly synthesized as a result of glucose metabolism. Based on the reference glucose-d_7 spectrum in the νC-^{2}H stretching range (Fig. 2, top spectrum) and the deuterated protein spectra reported in the literature (peaking at approx. 2185 cm^{-1}, Yasuda et al., 2021; Zhang et al., 2019), the band intensity profile suggests that the unmetabolized glucose signal is stronger in the Cu treatment sample and that the deuterated protein signal is stronger in the Control sample. This is also confirmed by analysis of difference spectra, where the reference glucose-d_7 spectrum was used for a scaled subtraction from the spectra of hyphae in the control and the Cu treatments (SI Fig. 6). However, since the band fitting indicates shifts in the spectral band positions compared to the pure glucose spectrum, this assignment remains tentative. The different spectral profiles can also indicate changes in overall glucose metabolism and the νC-^{2}H signal stemming from a different set of molecules, predominantly proteins/nucleic acids (Yasuda et al., 2021; Zhang et al., 2019) or them being in different environments, such as different cytosolic pH (Azevedo et al., 2016) in Cu *vs* Control treatments. Unfortunately, the signal-to-noise ratio and the intensity of the νC-^{2}H bands was too low, particularly in the spectra of hyphae from the Cu treatment, to achieve a reliable fit from the other time points.

To further estimate how the glucose-d_7 metabolism rates in *P. cf. subviscida* hyphae are affected by the presence of Cu in the system, we calculated the νC-^{2}H/δC-H band area intensity ratio in the spectra of hyphae recorded in 4 replicate chips during 46 h after the treatment addition (Fig. 3). The ratio indicates relative enrichment of cell constituting compounds with deuterium and is proportional to glucose anabolic metabolism rates. It corresponds well with the non-irradiated hyphal growth rates measured as elongation per time along the chip channels (SI Fig. 7 a). Of note, while total elongation is larger in the radiation-affected hyphae (SI Fig. 7 b), which is likely due to random hyphal selection for monitoring and high variance in the growth rates of individual hyphae, the growth rates of the laser-exposed hyphae were reduced after 20 h and remained unaffected in the non-exposed ones. As expected, the presence of excess Cu further slowed down and eventually halted both the growth and glucose metabolism of *P. cf. subviscida* hyphae, with a significant difference in the νC-^{2}H/δC-H band intensity

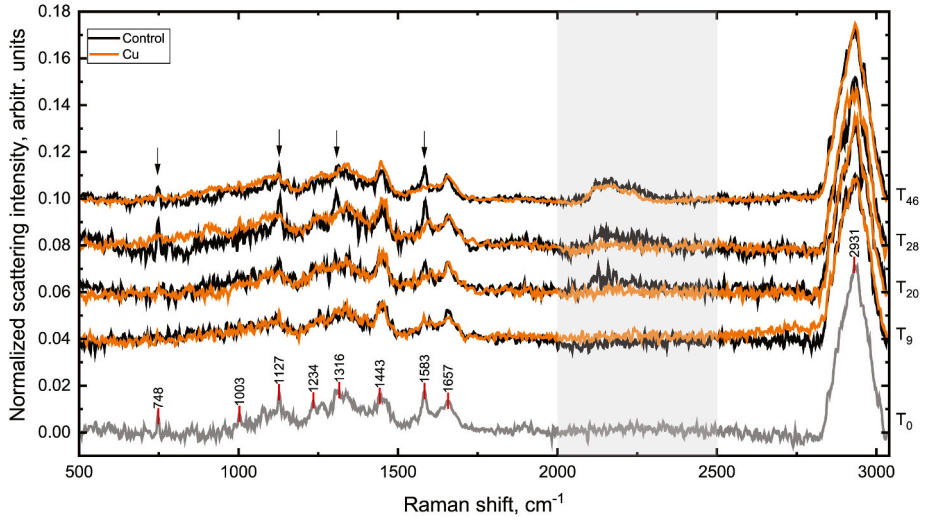

Fig. 1. Vector normalized Raman spectra of *P. cf. subviscida* hyphae at subsequent time points after addition of glucose-d_7 in control (black) and Cu (orange) treatments (x5 spectra averaged). Arrows mark the decreasing intensity of cytochrome *c* bands in Cu affected hyphae, and the grey area highlights the νC-^{2}H spectral range shown in Fig. 2. Of note, at 9 h, the cytochrome *c* associated bands are weaker in the spectrum of the control treatment compared to other time points, likely due to phenotypical (metabolic activity) heterogeneity effect across individual hyphae, and the fact that each time point sampled a different set of individual hyphae. The spectra recorded at the different time points are shifted vertically for clarity. (For interpretation of the references to colour in this figure legend, the reader is referred to the Web version of this article.)

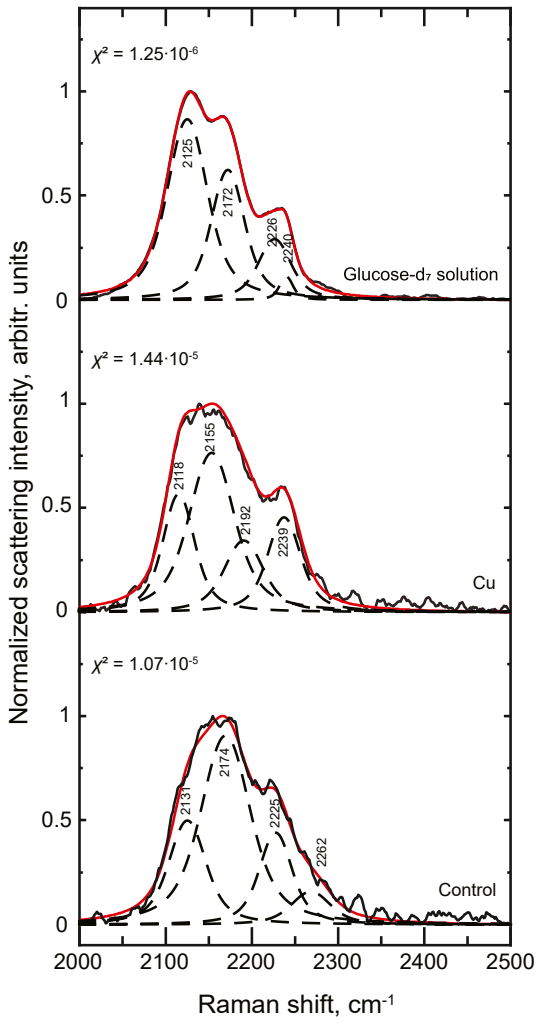

Fig. 2. Min-max normalized νC-^{2}H spectral range in the Raman spectra of glucose-d_7 in aqueous solution (top), and fungal hyphae after 46 h in control (bottom) and Cu (middle) treatments. The dashed lines show Voigt contours fitted to the bands and the red outline visualizes the overall fit, characterized by the goodness-of-fit parameter χ^2. The spectra and their fits are shifted vertically for clarity. (For interpretation of the references to colour in this figure legend, the reader is referred to the Web version of this article.)

ratio between the two treatments ($p < 0.001$).

In addition to the single point measurements of hyphal tips in the chips, we performed multispectral mapping in order to determine the distribution of deuterium-associated and other compounds in the *P. cf. subviscida* hyphae (SI Figs. 8 and 9). However, when subjected to laser exposure for a prolonged period of time when collecting the multiple spectra in the maps, the hyphae tended to move out of focus in the chip channels during the measurement or were ruptured, resulting in cytoplasm spillage. Sensitivity to the laser radiation limited the exposure, and thus the quality of the spectra in terms of signal-to-noise ratio that could be achieved and the number of data points that could be collected. While overall contours of the imaged cells were identified, mainly via spectral signature of proteins (amide I band at 1657 cm^{-1}), the noisy signal and the small number of data points restricted the information that could be extracted from the spectral maps (SI Figs. 8 and 9), and no clear conclusions regarding distribution of ^{2}H enriched biomolecular compounds within the hyphae could be made.

In order to avoid these radiation effects, we employed, for the first time, the SRS imaging technique, which allows for much faster signal acquisition and higher sensitivity due to the increased intensity of the collected Raman signal. This is achieved by using two synchronized

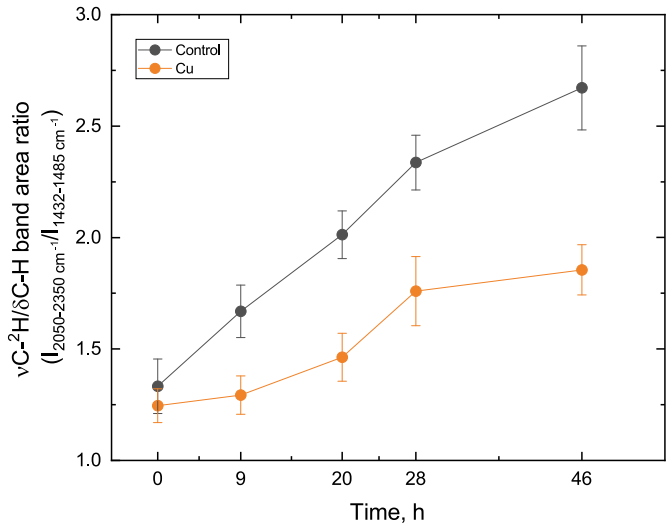

Fig. 3. Hyphal ^{2}H incorporation rates in the control (black) and Cu (orange) treatment, calculated as the νC-^{2}H to δC-H band area intensity ratio (integral limits 2050-2350 cm^{-1} for νC-^{2}H band and 1432-1485 cm^{-1} for δC-H band), representing relative deuterium enrichment in the hyphae. Error bars show standard error ($n = 21$-28). (For interpretation of the references to colour in this figure legend, the reader is referred to the Web version of this article.)

lasers (pump and Stokes) to coherently drive specific vibrational transitions, greatly amplifying the Raman signal and reducing the background noise compared to spontaneous Raman scattering (Lin et al., 2025). Importantly, the pixel dwell time could be reduced to 177 μs, compared to 32 s for spontaneous Raman mapping. The SRS imaging was performed on living hyphae in newly prepared chips, both before and 1 day after glucose-d_7 and Cu with glucose-d_7 treatment addition (as above). Spectral image stacks were acquired at the most intense νC-H spectral band (2932 cm^{-1}) and at several selected wavenumbers of the νC-^{2}H spectral range (2130, 2154, 2170 and 2207 cm^{-1}, SI Fig. 10). Under SRS conditions we could map much larger areas and at the same time reduce the mapping step size to 120 or 150 nm (oversampling) to improve the signal-to-noise ratio.

Representative microscopic and SRS scans of untreated (control) and Cu-exposed samples are presented in Fig. 4. Panels a and a′ show wide-field images of hyphae extending from the chip channel into the diamond shaped chamber. In panel a, three hyphae are growing in the imaging plane of the microscope. In contrast, panel a′ displays two hyphae oriented vertically along the z-axis, one positioned above the other, resulting in an increased SRS signal observed in panel b′. Red boxes highlight the regions selected for SRS imaging (panels b–f, b'–f').

The νC–H vibrational mode produces a strong signal in the SRS images (panels b and b′), which enabled effective denoising as described in the Materials and Methods section and provided clear insights into hyphal morphology. Notably, high-intensity circular spots were observed along the hyphae in both treatment conditions, indicated by yellow arrows. Meanwhile, in the Cu affected hyphae (b'), a consistent decrease in νC–H intensity within well-defined, round intracellular structures along the hyphae can be seen, as marked with magenta arrows. This trend was observed across several replicate hyphae as early as 7 h after Cu treatment addition (SI Fig. 11).

The intensity of νC-^{2}H bands in panels c-e, c'-e' was too low to reliably identify differences in the band structure across treatments. Denoising did not improve the signal sufficiently and was not applied to the scans. However, it can be observed that 24 h after label addition, the SRS signal intensities that indicate the distribution of deuterium-associated compounds, are the highest near the hyphal edges, providing spatially resolved information about glucose-d_7 incorporation into the cell. In order to confirm that the weak signals observed in these

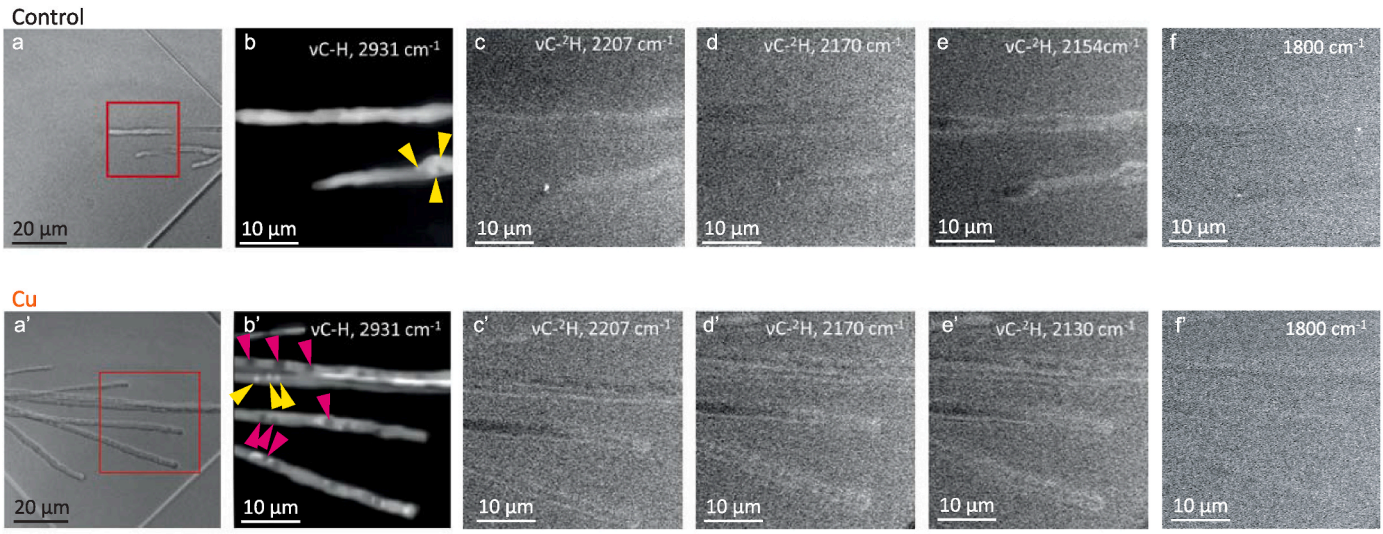

Fig. 4. Optical (a, a') and SRS (b - f, b' - f') images of *P. cf. subviscida* hyphae collected at different Raman wavenumbers 1 day after addition of glucose-d_7 in a control (a – f, pixel size in SRS images 120 nm) or glucose-d_7 together with $CuSO_4 \bullet 5H_2O$ in the Cu (a' – f', pixel size in SRS images 150 nm) treatment. Yellow arrows in the νC-H images of hyphae in both control and Cu treatments mark some of the higher signal intensity regions, tentatively identified as lipid droplets, while magenta arrows in the image of hyphae in the Cu treatment - the lower signal intensity regions, putative vacuoles. Of note, the sample shifted slightly during the measurement of Cu-exposed sample, which is why the hyphae in the image c' seem slightly shifted compared to d' and e'. SRS images in f and f' were recorded at an off-resonance 1800 cm^{-1} Raman shift, where no scattering signal from the sample is expected. (For interpretation of the references to colour in this figure legend, the reader is referred to the Web version of this article.)

images are not stemming from non-Raman scattering associated effects, such as transient absorption or cross-phase modulation (Zhang et al., 2014), we also recorded SRS images at 1800 cm^{-1} (panels f and f' in Fig. 4), where no Raman scattering was expected to occur in our samples. While some background signals can be discerned around the hyphae, they are significantly weaker than the ones observed in the C-^{2}H SRS images, confirming that the latter stem from real SRS signals. The same off-resonance check was applied to the SRS images of SI Fig. 11. Of note, no radiation damage effects were observed for the hyphae imaged via SRS microscopy.

4. Discussion

4.1. SIP-Raman microspectroscopy as a tool for soil fungal metabolism analysis

SIP-Raman microspectroscopy has been increasingly used for studying primary metabolic activity of microorganisms in different settings (No et al., 2022; Alcolombri et al., 2022; Wang et al., 2016), but its applications to the analysis of filamentous fungi has so far been limited. This is likely due to the complexity and heterogeneity of these organisms, where functionally diverse hyphae in the fungal mycelium can differ in both their metabolic activity (Op De Beeck et al., 2020) and biochemical composition. Differences can further be observed along individual hyphae, with apexes often being more active than subapical or older regions. Yasuda et al. has demonstrated the potential of SIP-Raman microspectroscopy for tracing glucose metabolism in hyphae of soil fungus *A. nidulans*, as well as visualizing the metabolic products across the hyphal tips (Yasuda et al., 2021) Here, we further show that the approach can be used to trace hyphal metabolic response to environmental stressors. We additionally employed soil chips, which allow retaining the growing fungal culture closed and sterile even for prolonged periods of time (e.g., for slow growing fungi), while at the same time multiple chip channels provide an internal replication system. We found, consistent with our hypothesis, that excess Cu interferes with the growth and hyphal metabolic activity of fungus *P. cf. subviscida*, which is reflected in glucose uptake rates as represented by the relative intensity of the νC-^{2}H band. While individual hyphae could not be followed over time due to radiation damage (refer to Results and the discussion below), we interpret the results from individual replicate hyphae as overall organismal response. The variance of the relative νC-^{2}H band intensity (Fig. 2), although influenced by the signal-to-noise ratio and spatial variation of ^{2}H enrichment along the hyphae not captured in single point measurements, is also meaningful and reflects differences in the glucose metabolic activity among individual cells. Such phenotypical heterogeneity has been reported in filamentous microorganisms, including fungi (Hewitt et al., 2016; Op De Beeck et al., 2020; Zacchetti et al., 2018), and can be observed both among individual cells and along a single compartmentalized hypha (SI Fig. 12). It is higher in control treatments, where stronger differences in metabolic activity of hyphae are expected given spatial organization of growth and function in filamentous fungi (Zacchetti et al., 2018). Meanwhile, decreased relative νC-^{2}H band intensity together with increased uniformity across hyphae suggests systemic suppression of glucose metabolic activity as a response to excess Cu.

Raman microspectroscopy and spectral analysis further enabled us to extract information about biochemical cellular responses to stress. While providing only limited chemical resolution, differences in the relative intensities and peak positions of the νC-^{2}H bands in *P. cf. subviscida* hyphae across control and Cu treatments suggest alterations in glucose processing and its incorporation into newly synthesized macromolecules (e.g., proteins/nucleic acids). Previous studies performed isolation of the newly synthesized cellular compounds enriched in deuterium and used their Raman spectra as reference for applying linear spectral unmixing protocols for better insights into the chemistry of glucose metabolism in mammalian cells (Zhang et al., 2019). While this approach in fungi is complicated by their filamentous growth, where different parts of hyphae can be heterogeneous in terms of their growth stage and function, and also because of the rigid chitinous cell wall (Bridge et al., 2004), in the future, this could also be performed for improved band assignment and better understanding of hyphal biochemistry and metabolic processes under Cu stress.

Furthermore, the intensity decrease and the disappearance of characteristic resonant Raman bands related to cytochrome *c* in the Cu affected *P. cf. subviscida* hyphae indicates impaired production/function of that protein. Yasuda et al. also observed a decrease in cytochrome *c*

Raman bands in the fungus *A. nidulans*, and assigned it to photobleaching (Yasuda et al., 2021). We rule out photobleaching in our case, as cytochrome *c* bands remained unaffected in the analysed hyphae in the control treatment, and spectra were mostly collected on different hyphae at each time point. Within eukaryotic cells, cytochrome *c* is located in mitochondria, where it is responsible for electron transfer in respiratory processes (Garrido et al., 2006). Mitochondria have been shown to be one of the earliest organelles to be affected by excess Cu, even in the hyphae of Cu resistant fungi (Krumova et al., 2012). Under stress, the mitochondrial cytochrome can be released into the cytosol, where it binds with other proteins to initiate cellular apoptosis (Ow et al., 2008), which could lead to changes in resonance conditions and overall spectral signature of the compound and result in disappearance of the characteristic cytochrome *c* bands in the Raman spectra. Thus, disappearance of cytochrome *c* spectral bands in the *P. cf. subviscida* hyphae affected by Cu can indicate interference in the mitochondrial function and, potentially, initiation of cell death.

4.2. Raman chemical mapping

Multispectral chemical mapping of living fungal hyphae in soil chips using spontaneous Raman microspectroscopy remains challenging. This is largely due to the combined effects of radiation damage, long acquisition times, and spatial instability of living hyphae under prolonged laser exposure (in this study typically 32 s per pixel). Acquiring a multispectral Raman map of a single hyphal tip required several to tens of hours, depending on the mapping area, spatial and spectral resolution, and acquisition parameters. In this work, in addition to direct radiation damage to the hyphae due to prolonged excitation laser exposure, hyphal displacement within the chip channels - either as part of a cellular response or physical effects due to localized heating caused by laser exposure - complicated high-resolution mapping. Hyphae often drifted out of the laser's focal plane or moved outside the predefined mapping area, compromising data quality. In the future, this could potentially be solved by designing and fabricating chips with channels of lower height and width. While overall contours of the imaged cells were identified in successfully recorded maps via distribution of amide I and, 1 day after glucose-d_7 addition, via C-^{2}H integral intensity values, no spatially specific information could be extracted.

Instead, as a proof of concept, we demonstrate that SRS microscopy and single frequency mapping of νC-^{2}H and other Raman signature bands enables non-destructive chemical imaging of individual or multiple hyphae over larger areas and requiring much shorter total acquisition times. Compared to spontaneous Raman, SRS offers higher sensitivity and faster imaging (Lin et al., 2025). Specifically, when collecting spectral maps in this work the exposure time per pixel for SRS was 5 orders of magnitude shorter than for spontaneous Raman scattering. This also resulted in minimized radiation damage effects.

Consistent with previous findings by Yasuda et al. (2021), the SRS images show that the νC–^{2}H signal - after ~1 day of incubation with glucose-d_7 - is predominantly localized along the inner edges of *P. cf. subviscida* hyphae, regardless of treatment, corresponding with glucose transport from the medium into the cell via the cell wall. We also show that mapping the intense νC-H spectral band can provide additional morpho-chemical information. High νC-H intensity circular spots are likely lipid droplets. In the Cu-treated samples, SRS images of hyphae show a consistent decrease in νC–H intensity within well-defined, round intracellular structures along the hyphae. The contrast of the optical images was not sufficient to distinguish these bodies, but they are likely vacuoles – liquid-filled compartments, which form as a stress response to Cu in fungi (Krumova et al., 2012).

While these pilot results demonstrate the benefits of using SRS for chemical mapping of fungal hyphae, applications in combination with soil chips require further improvements. We were unable to optimally accommodate the chips bonded within glass-bottomed Petri dishes on the sample stage of the SRS microscope system. This was due to both space limitations and the fact that the optical path through plastic, air gaps, PDMS, and liquid-filled chip channels introduced refractive index mismatches and scattering, which led to strong SRS signal attenuation. We thus conducted measurements with the chips removed from the Petri dishes; however, this compromised sterility and limited the time window available for the imaging.

Even outside the plate, signal quality remained suboptimal, limiting the possibilities for imaging at lower intensity Raman spectral bands. In transmission mode, scattering within the PDMS matrix reduced signal intensity and sensitivity, particularly for the weaker C–^{2}H bands. As a result, we were unable to obtain contrast between the different components in the spectral region. In epi-mode, weak backscattered SRS signal was also insufficient for obtaining chemical contrast. Therefore, for future SRS applications, thinner PDMS chips for improved optical clarity, and the possibility to enclose the entrance with fungal inoculum for maintaining sterility, would be necessary for reliable time-resolved chemical imaging *in situ*.

4.3. Radiation damage effects

An important issue to address when using SIP-Raman microspectroscopy for fungal primary metabolism analysis is radiation damage from the intense radiation of the excitation laser. In this work, even using the relatively low laser power and limited exposure times, we observed radiation damage effects on the hyphae of fungus *P. cf. subviscida*. Of note, the extent of the damage was dependent on cell morphology (data not shown), with thinner exploring hyphae typically being more susceptible and displaying immediate effects such as cytoplasm spillage. Thicker trunk hyphae were typically less affected, but suffered cumulative damage effects (SI Fig. 5), with reduced or halted growth after a few subsequent irradiation events at the different time points. Cu affected hyphae were also more sensitive to laser exposure (SI Fig. 5), suggesting lower capacity of the fungus to cope with two simultaneous stressors. While radiation damage poses a challenge to characterize individual hyphal metabolic processes, Raman spectra collected on different cells at each data points provided valuable information about organismal responses, while variation in the spectral signatures indicate hyphal functional heterogeneity. Of note, different fungal species are likely to have different thresholds for radiation damage, requiring species-specific optimization of experimental parameters for minimizing the effect and maximizing spectral insights into the metabolic processes at both cellular and organismal scales.

On the other hand, SRS microscopy is a promising approach for chemical imaging of the biochemical compound distribution along the fungal hyphae. The increased sensitivity and significantly shorter acquisition time were sufficient to decrease radiation damage effects in our system. While further experiments are necessary to confirm this, as well as improvements to the soil chip design as discussed above, in the future, the method could provide chemically specific and spatially resolved information about fungal metabolic processes *in situ* at hyphal scale.

5. Conclusions

In this work, we demonstrated that SIP-Raman microspectroscopy can be used to trace glucose metabolism and stress-associated metabolic activity response in filamentous fungi. Despite the challenges related to radiation damage from the excitation laser in spontaneous Raman, we were able to obtain valuable information about overall organismal response and level of hyphal functional heterogeneity. Specifically, fungus *P. cf. subviscida* showed reduced glucose uptake as well as growth rates when exposed to excess Cu in the environment. In addition, reduction in cytochrome *c* signal in the Raman spectra of the fungal hyphae suggests interference in hyphal mitochondrial function and initiation of apoptotic processes. Increased uniformity across hyphae further indicates a systemic metabolic response.

For spatially-resolved information, SRS microscopy enabled faster chemical mapping with improved sensitivity and reduced radiation damage effects compared to spontaneous Raman scattering based approach. Localization of νC–^{2}H signal at the inner edge of the *P. cf. subviscida* hyphae and decline in νC–H intensity in vacuole-like structures under Cu stress demonstrate its usefulness for visualizing morphochemical responses. However, for applications in combination with soil chips, optically optimized chip design and improved integration into the imaging system are essential for future *in situ* studies.

All in all, SIP-Raman and SRS microspectroscopy are powerful approaches that, with further developments, have potential for tracing metabolic dynamics in soil filamentous fungi, particularly for better understanding of stress physiology at the hyphal scale.

CRediT authorship contribution statement

Milda Pucetaite: Writing – original draft, Visualization, Methodology, Investigation, Funding acquisition, Formal analysis, Conceptualization. **Paola M. Mafla-Endara:** Writing – review & editing, Investigation. **Yitsully G. González:** Writing – review & editing, Methodology. **Hanbang Zou:** Writing – review & editing, Methodology. **Robert W. Schmidt:** Writing – review & editing, Methodology. **Freek Ariese:** Writing – review & editing, Methodology, Conceptualization. **Edith C. Hammer:** Writing – review & editing, Methodology, Funding acquisition.

Declaration of competing interest

The authors declare that they have no known competing financial interests or personal relationships that could have appeared to influence the work reported in this paper.

Acknowledgements

The authors acknowledge financial support from the Swedish Research Council to Milda Pucetaite (grant no 2021-03897) and the Foundation for Strategic Research to Edith Hammer (grant no. SSF FFL 18-0089). We further acknowledge financial support from NanoLund for fabrication of the microfluidic chip masters and from LaserLaB Europe (EU Horizon 2020 grant # 871124) for supporting the SRS experiments at LaserLaB Amsterdam (access proposal ID: 26520). Thank you to Merel C. Konings for her help and support with operating the SRS system.

Raman microspectroscopy measurements were performed at the Microscopy Facility at the Department of Biology, Lund University. Finally, Milda Pucetaite is grateful to prof. Toby Kiers and Dr. Vasilios Kokkoris at Vrije Universiteit Amsterdam for hosting her as a guest researcher during and beyond the course of this work.

While preparing this manuscript, our co-author, colleague, and supervisor Freek Ariese sadly passed away. We acknowledge his invaluable contributions to this work in particular and to the scientific community at large. We are deeply grateful for his support, guidance, and friendship.

Appendix A. Supplementary data

Supplementary data to this article can be found online at https://doi.org/10.1016/j.funbio.2026.101749.

References

Alcolombri, U., Pioli, R., Stocker, R., Berry, D., 2022. Single-cell stable isotope probing in microbial ecology. ISME Commun 2, 1–9. https://doi.org/10.1038/s43705-022-00142-3.

Aleklett, K., Kiers, E.T., Ohlsson, P., Shimizu, T.S., Caldas, V.E., Hammer, E.C., 2018. Build your own soil: exploring microfluidics to create microbial habitat structures. ISME J. 12, 312–319. https://doi.org/10.1038/ismej.2017.184.

Arellano-Caicedo, C., Ohlsson, P., Bengtsson, M., Beech, J.P., Hammer, E.C., 2021. Habitat geometry in artificial microstructure affects bacterial and fungal growth, interactions, and substrate degradation. Commun. Biol. 4, 1–11. https://doi.org/10.1038/s42003-021-02736-4.

Azevedo, M.M., Guimarães-Soares, L., Pascoal, C., Cássio, F., 2016. Copper and zinc affect the activity of plasma membrane H+-ATPase and thiol content in aquatic fungi. Microbiology 162, 740–747. https://doi.org/10.1099/mic.0.000262.

Berry, D., Mader, E., Lee, T.K., Woebken, D., Wang, Y., Zhu, D., Palatinszky, M., Schintlmeister, A., Schmid, M.C., Hanson, B.T., Shterzer, N., Mizrahi, I., Rauch, I., Decker, T., Bocklitz, T., Popp, J., Gibson, C.M., Fowler, P.W., Huang, W.E., Wagner, M., 2015. Tracking heavy water (D2O) incorporation for identifying and sorting active microbial cells. Proc. Natl. Acad. Sci. 112, E194–E203. https://doi.org/10.1073/pnas.1420406112.

Bölscher, T., Vogel, C., Olagoke, F.K., Meurer, K.H.E., Herrmann, A.M., Colombi, T., Brunn, M., Domeignoz-Horta, L.A., 2024. Beyond growth: the significance of non-growth anabolism for microbial carbon-use efficiency in the light of soil carbon stabilisation. Soil Biol. Biochem. 193, 109400. https://doi.org/10.1016/j.soilbio.2024.109400.

Bridge, P.D., Kokubun, T., Simmonds, M.S.J., 2004. Protein extraction from fungi. Methods Mol. Biol. Clifton NJ 244, 37–46. https://doi.org/10.1385/1-59259-655-x.

Butler, H.J., Ashton, L., Bird, B., Cinque, G., Curtis, K., Dorney, J., Esmonde-White, K., Fullwood, N.J., Gardner, B., Martin-Hirsch, P.L., Walsh, M.J., McAinsh, M.R., Stone, N., Martin, F.L., 2016. Using Raman spectroscopy to characterize biological materials. Nat. Protoc. 11, 664–687. https://doi.org/10.1038/nprot.2016.036.

Calabrese, F., Stryhanyuk, H., Moraru, C., Schlömann, M., Wick, L.Y., Richnow, H.H., Musat, F., Musat, N., 2021. Metabolic history and metabolic fitness as drivers of anabolic heterogeneity in isogenic microbial populations. Environ. Microbiol. 23, 6764–6776. https://doi.org/10.1111/1462-2920.15756.

Camenzind, T., Vonhoegen, D., Elshal, A., Oliva, R.L., Whitehead, L., Martin, C., Hempel, S., Tebbe, C.C., Rillig, M.C., Thiele-Bruhn, S., Finn, D., 2025. What are all these soil fungi doing? Complex carbon use ability as a predictive trait for fungal community functions. https://doi.org/10.1101/2025.07.11.664336.

Costa, B. de O., Nahas, E., 2012. Growth and enzymatic responses of phytopathogenic fungi to glucose in culture media and soil. Braz. J. Microbiol. 43, 332–340. https://doi.org/10.1590/S1517-83822012000100039.

Cui, L., Xin, Y., Yang, K., Li, H., Tan, F., Zhang, Y., Li, X., Zhu, Z., Yang, J., Kao, S.-J., Ren, B., Zhu, Y.-G., Musat, F., Musat, N., 2023. Live tracking metabolic networks and physiological responses within microbial assemblages at single-cell level. PNAS Nexus 2. https://doi.org/10.1093/pnasnexus/pgad006 pgad006.

Dabov, K., Foi, A., Katkovnik, V., Egiazarian, K., 2007. Image denoising by sparse 3-D transform-domain collaborative filtering. IEEE Trans. Image Process. 16, 2080–2095. https://doi.org/10.1109/TIP.2007.901238.

Chrimes, A.F., Khoshmanesh, K.R., Stoddart, P., Mitchell, A., Kalantar-zadeh, K., 2013. Microfluidics and Raman microscopy : current applications and future challenges. Chem. Soc. Rev. 42, 5880–5906. https://doi.org/10.1039/C3CS35515B.

Figueroa, B., Fu, W., Nguyen, T., Shin, K., Manifold, B., Wise, F., Fu, D., 2018. Broadband hyperspectral stimulated Raman scattering microscopy with a parabolic fiber amplifier source. Biomed. Opt. Express 9, 6116–6131. https://doi.org/10.1364/BOE.9.006116.

Fu, D., Holtom, G., Freudiger, C., Zhang, X., Xie, X.S., 2013. Hyperspectral imaging with stimulated raman scattering by chirped femtosecond lasers. J. Phys. Chem. B 117, 4634–4640. https://doi.org/10.1021/jp308938t.

Gao, D., Huang, X., Tao, Y., 2016. A critical review of NanoSIMS in analysis of microbial metabolic activities at single-cell level. Crit. Rev. Biotechnol. 36, 884–890. https://doi.org/10.3109/07388551.2015.1057550.

Garrido, C., Galluzzi, L., Brunet, M., Puig, P.E., Didelot, C., Kroemer, G., 2006. Mechanisms of cytochrome c release from mitochondria. Cell Death Differ. 13, 1423–1433. https://doi.org/10.1038/sj.cdd.4401950.

Gimeno, A., Stanley, C.E., Ngamenie, Z., Hsung, M.-H., Walder, F., Schmieder, S.S., Bindschedler, S., Junier, P., Keller, B., Vogelgsang, S., 2021. A versatile microfluidic platform measures hyphal interactions between Fusarium graminearum and Clonostachys rosea in real-time. Commun. Biol. 4, 1–10. https://doi.org/10.1038/s42003-021-01767-1.

Hatzenpichler, R., Orphan, V.J., 2016. Detection of protein-synthesizing microorganisms in the environment via bioorthogonal noncanonical amino acid tagging (BONCAT). In: McGenity, T.J., Timmis, K.N., Nogales, B. (Eds.), Hydrocarbon and Lipid Microbiology Protocols: Single-Cell and Single-Molecule Methods. Springer, Berlin, Heidelberg, pp. 145–157. https://doi.org/10.1007/8623_2015_61.

Hatzenpichler, R., Krukenberg, V., Spietz, R.L., Jay, Z.J., 2020. Next-generation physiology approaches to study microbiome function at single cell level. Nat. Rev. Microbiol. 18, 241–256. https://doi.org/10.1038/s41579-020-0323-1.

Hewitt, S.K., Foster, D.S., Dyer, P.S., Avery, S.V., 2016. Phenotypic heterogeneity in fungi: importance and methodology. Fungal Biol. Rev. 30, 176–184. https://doi.org/10.1016/j.fbr.2016.09.002.

Highley, T.L., 1973. Influence of carbon source on cellulase activity of white-rot and brown-rot fungi. Wood Fiber Sci. 5, 50–58.

Hou, Z., Tuo, J., Ma, X., Huo, Y.-X., 2025. Recent advances in biosynthesis of non-canonical amino acids and their potentials in strain engineering. Results Eng. 25, 103641. https://doi.org/10.1016/j.rineng.2024.103641.

Imdahl, F., Vafadarnejad, E., Homberger, C., Saliba, A.-E., Vogel, J., 2020. Single-cell RNA-sequencing reports growth-condition-specific global transcriptomes of individual bacteria. Nat. Microbiol. 5, 1202–1206. https://doi.org/10.1038/s41564-020-0774-1.

Ivleva, N.P., Kubryk, P., Niessner, R., 2017. Raman microspectroscopy, surface-enhanced Raman scattering microspectroscopy, and stable-isotope Raman microspectroscopy

for biofilm characterization. Anal. Bioanal. Chem. 409, 4353–4375. https://doi.org/10.1007/s00216-017-0303-0.
Joux, F., Lebaron, P., 2000. Use of fluorescent probes to assess physiological functions of bacteriaat single-cell level. Microbes Infect 2, 1523–1535. https://doi.org/10.1016/S1286-4579(00)01307-1.
Krumova, E.Ts, Stoitsova, S.R., Paunova-Krasteva, T.S., Pashova, S.B., Angelova, M.B., 2012. Copper stress and filamentous fungus Humicola lutea 103 — ultrastructural changes and activities of key metabolic enzymes. Can. J. Microbiol. 58, 1335–1343. https://doi.org/10.1139/w2012-112.
Lin, H., Seitz, S., Tan, Y., Lugagne, J.-B., Wang, L., Ding, G., He, H., Rauwolf, T.J., Dunlop, M.J., Connor, J.H., Porco, J.A., Tian, L., Cheng, J.-X., 2025. Label-free nanoscopy of cell metabolism by ultrasensitive reweighted visible stimulated Raman scattering. Nat. Methods 1–11. https://doi.org/10.1038/s41592-024-02575-1.
Mafla-Endara, P.M., Arellano-Caicedo, C., Aleklett, K., Pucetaite, M., Ohlsson, P., Hammer, E.C., 2021. Microfluidic chips provide visual access to in situ soil ecology. Commun. Biol. 4, 1–12. https://doi.org/10.1038/s42003-021-02379-5.
Mafla-Endara, P.M., Meklesh, V., Beech, J.P., Ohlsson, P., Pucetaite, M., Hammer, E.C., 2023. Exposure to polystyrene nanoplastics reduces bacterial and fungal biomass in microfabricated soil models. Sci. Total Environ. 904, 166503. https://doi.org/10.1016/j.scitotenv.2023.166503.
Mäkinen, Y., Azzari, L., Foi, A., 2020. Collaborative filtering of correlated noise: exact transform-domain variance for improved shrinkage and patch matching. IEEE Trans. Image Process. 29, 8339–8354. https://doi.org/10.1109/TIP.2020.3014721.
Mucha, J., 2011. Changes in hyphal morphology and activity of phenoloxidases during interactions between selected ectomycorrhizal fungi and two species of Trichoderma. Antonie Leeuwenhoek 100, 155–160. https://doi.org/10.1007/s10482-011-9556-3.
Nandakumar, P., Kovalev, A., Volkmer, A., 2009. Vibrational imaging based on stimulated Raman scattering microscopy. New J. Phys. 11, 033026. https://doi.org/10.1088/1367-2630/11/3/033026.
No, J.H., Nishu, S.D., Hong, J.-K., Lyou, E.S., Kim, M.S., Wee, G.N., Lee, T.K., 2022. Raman-Deuterium isotope probing and metagenomics reveal the drought tolerance of the soil microbiome and its promotion of plant growth. mSystems 7. https://doi.org/10.1128/msystems.01249-21 e01249-21.
Omelchenko, A.N., Okotrub, K.A., Surovtsev, N.V., 2023. Raman spectroscopy of yeast cells cultured on a deuterated substrate. Spectrochim. Acta. A. Mol. Biomol. Spectrosc. 303, 123262. https://doi.org/10.1016/j.saa.2023.123262.
Omelchenko, A.N., Okotrub, K.A., Igonina, T.N., Rakhmanova, T.A., Okotrub, S.V., Rozhkova, I.N., Kozeneva, V.S., Amstislavsky, S.Ya, Surovtsev, N.V., 2025. Probing metabolism in mouse embryos using Raman spectroscopy and deuterium tags. Spectrochim. Acta. A. Mol. Biomol. Spectrosc. 325, 125044. https://doi.org/10.1016/j.saa.2024.125044.
Op De Beeck, M., Troein, C., Siregar, S., Gentile, L., Abbondanza, G., Peterson, C., Persson, P., Tunlid, A., 2020. Regulation of fungal decomposition at single-cell level. ISME J. 14, 896–905. https://doi.org/10.1038/s41396-019-0583-9.
Ow, Y.-L.P., Green, D.R., Hao, Z., Mak, T.W., 2008. Cytochrome c: functions beyond respiration. Nat. Rev. Mol. Cell Biol. 9, 532–542. https://doi.org/10.1038/nrm2434.
Pucetaite, M., Ohlsson, P., Persson, P., Hammer, E., 2021. Shining new light into soil systems: spectroscopy in microfluidic soil chips reveals microbial biogeochemistry. Soil Biol. Biochem. 153, 108078. https://doi.org/10.1016/j.soilbio.2020.108078.
Redmile-Gordon, M.A., Brookes, P.C., Evershed, R.P., Goulding, K.W.T., Hirsch, P.R., 2014. Measuring the soil-microbial interface: extraction of extracellular polymeric substances (EPS) from soil biofilms. Soil Biol. Biochem. 72, 163–171. https://doi.org/10.1016/j.soilbio.2014.01.025.
Richter, F., Bindschedler, S., Calonne-Salmon, M., Declerck, S., Junier, P., Stanley, C.E., 2022. Fungi-on-a-Chip: microfluidic platforms for single-cell studies on fungi. FEMS Microbiol. Rev. 46. https://doi.org/10.1093/femsre/fuac039 fuac039.
Robinson, J.R., Isikhuemhen, O.S., Anike, F.N., 2021. Fungal–Metal interactions: a review of toxicity and homeostasis. J. Fungi 7, 225. https://doi.org/10.3390/jof7030225.
Rousk, J., Bååth, E., 2011. Growth of saprotrophic fungi and bacteria in soil. FEMS Microbiol. Ecol. 78, 17–30. https://doi.org/10.1111/j.1574-6941.2011.01106.x.
Schaible, G.A., Kohtz, A.J., Cliff, J., Hatzenpichler, R., 2022. Correlative SIP-FISH-Raman-SEM-NanoSIMS links identity, morphology, biochemistry, and physiology of environmental microbes. ISME Commun 2, 1–10. https://doi.org/10.1038/s43705-022-00134-3.
Schneider, C.A., Rasband, W.S., Eliceiri, K.W., 2012. NIH Image to ImageJ: 25 years of image analysis. Nat. Methods 9, 671–675. https://doi.org/10.1038/nmeth.2089.
Stanley, E., C, Grossmann, G., Solvas, X.C. i, deMelloA, J., 2016. Soil-on-a-Chip: microfluidic platforms for environmental organismal studies. Lab Chip 16, 228–241. https://doi.org/10.1039/C5LC01285F.
Toplak, M., Birarda, G., Read, S., Sandt, C., Rosendahl, S.M., Vaccari, L., Demšar, J., Borondics, F., 2017. Infrared Orange: connecting hyperspectral data with machine learning. Synchrotron Radiat. News 30, 40–45. https://doi.org/10.1080/08940886.2017.1338424.
Toplak, M., Read, S.T., Sandt, C., Borondics, F., 2021. Quasar: easy machine learning for biospectroscopy. Cells 10, 2300. https://doi.org/10.3390/cells10092300.
van Haasterecht, L., Zada, L., Schmidt, R.W., de Bakker, E., Barbé, E., Leslie, H.A., Vethaak, A.D., Gibbs, S., de Boer, J.F., Niessen, F.B., van Zuijlen, P.P.M., Groot, M.L., Ariese, F., 2020. Label-free stimulated Raman scattering imaging reveals silicone breast implant material in tissue. J. Biophot. 13, e201960197. https://doi.org/10.1002/jbio.201960197.
Wang, Y., Song, Y., Tao, Y., Muhamadali, H., Goodacre, R., Zhou, N.-Y., Preston, G.M., Xu, J., Huang, W.E., 2016. Reverse and multiple stable isotope probing to Study bacterial metabolism and interactions at the single cell level. Anal. Chem. 88, 9443–9450. https://doi.org/10.1021/acs.analchem.6b01602.
Würthwein, T., Lüpken, N.M., Irwin, N., Fallnich, C., 2020. Mitigating cross-phase modulation artifacts in femtosecond stimulated Raman scattering. J. Raman Spectrosc. 51, 2265–2271. https://doi.org/10.1002/jrs.5958.
Xiong, B.-J., Stanley, C.E., Dusny, C., Schlosser, D., Harms, H., Wick, L.Y., 2022. pH distribution along growing fungal hyphae at microscale. J. Fungi 8, 599. https://doi.org/10.3390/jof8060599.
Xu, J., Zhu, D., Ibrahim, A.D., Allen, C.C.R., Gibson, C.M., Fowler, P.W., Song, Y., Huang, W.E., 2017. Raman deuterium isotope probing reveals microbial metabolism at the single-cell level. Anal. Chem. 89, 13305–13312. https://doi.org/10.1021/acs.analchem.7b03461.
Yasuda, M., Takeshita, N., Shigeto, S., 2021. Deuterium-labeled Raman tracking of glucose accumulation and protein metabolic dynamics in Aspergillus nidulans hyphal tips. Sci. Rep. 11, 1279. https://doi.org/10.1038/s41598-020-80270-9.
Zacchetti, B., Wösten, H.A.B., Claessen, D., 2018. Multiscale heterogeneity in filamentous microbes. Biotechnol. Adv. 36, 2138–2149. https://doi.org/10.1016/j.biotechadv.2018.10.002.
Zada, L., Fokker, B., Leslie, H.A., Vethaak, A.D., de Boer, J.F., Ariese, F., 2021. Stimulated Raman scattering simulation for imaging optimization. J. Eur. Opt. Soc.-Rapid Publ. 17, 10. https://doi.org/10.1186/s41476-021-00155-w.
Zhang, D., Wang, P., Slipchenko, M.N., Cheng, J.-X., 2014. Fast vibrational imaging of single cells and tissues by stimulated raman scattering microscopy. Acc. Chem. Res. 47, 2282–2290. https://doi.org/10.1021/ar400331q.
Zhang, L., Shi, L., Shen, Y., Miao, Y., Wei, M., Qian, N., Liu, Y., Min, W., 2019. Spectral tracing of deuterium for imaging glucose metabolism. Nat. Biomed. Eng. 3, 402–413. https://doi.org/10.1038/s41551-019-0393-4.